



Enhanced photocatalytic NO_x decomposition of visible-light responsive F-TiO₂/(N,C)-TiO₂ by charge transfer between F-TiO₂ and (N,C)-TiO₂ through their doping levels

Shio Komatsuda^a, Yusuke Asakura^a, Junie Jhon M. Vequizo^b, Akira Yamakata^b, Shu Yin^{a,*}

^a Institute of Multidisciplinary Research for Advanced Materials, Tohoku University, 2-1-1 Katahira, Aobaku, Sendai, 980-8577, Japan

^b Graduate School of Engineering, Toyota Technological Institute, 2-12-1 Hisakata, Tempaku, Nagoya, 468-8511, Japan



ARTICLE INFO

Keywords:
Composites
Photocatalytic deNO_x
Charge transfer
Doping level
Transient absorption

ABSTRACT

Composite type photocatalyst F-TiO₂/(N,C)-TiO₂ consisted of anatase-type TiO₂ with fluorine-doping (F-TiO₂) and TiO₂ with nitrogen and carbon-doping ((N,C)-TiO₂) was prepared by simple physical mixing to exhibit higher visible-light responsive photocatalytic nitrogen oxide (NO_x) decomposition activity than those of F-TiO₂ and (N,C)-TiO₂. Transient absorption measurement clarified that the composite possessed longer carrier lifetime compared to that of each material (F-TiO₂ or (N,C)-TiO₂), resulting in higher photocatalytic activity. In the composite, photoexcited holes and electrons, which are not in impurity level but in valence and conduction band, respectively, should photocatalytically decompose NO_x , judging from the redox potential of O_2/O_2^- and the band positions of F-TiO₂ and (N,C)-TiO₂. The mechanism for higher visible-light photocatalytic activity, or longer carrier lifetime can be explained by charge transfer between F-TiO₂ and (N,C)-TiO₂ through their impurity levels. The charge transfer should make photoexcited carries spatially separated to enhance the photocatalytic activity.

1. Introduction

Utilization of photocatalysts is one of the way for solution of recent energy and environment problems, because they can induce redox reactions under solar light which almost permanently reaches to the earth [1]. The redox reactions by photocatalysts can lead to many applications including self-cleaning, decomposition of substance and water-splitting [2,3]. Titanium dioxide (TiO₂) is one of the metal oxide semiconductors with high photocatalytic activity [4,5]. Because TiO₂ is chemical and physical stable, low-cost and easy to be synthesized, it was widely studied and practically applied. Among various crystal structure of TiO₂, anatase type TiO₂ has been known as an excellent photocatalyst. However, band gap of anatase-type TiO₂ is too wide (~3.2 eV), and anatase-type TiO₂ possesses no visible-light photoresponsivity [6]. Therefore, many efforts have been paid for creation of visible-light responsivity in TiO₂.

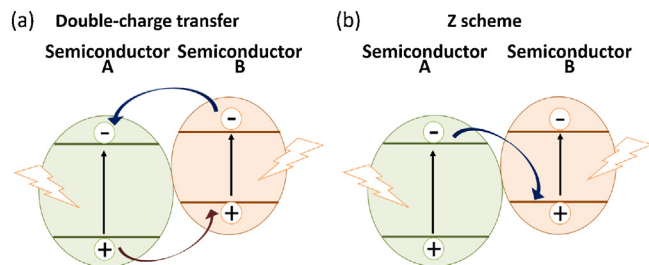
Some elements have been doped to TiO₂ to realize visible-light photoresponsivity [7–11]. Recently, much attention has been given to anion doping including nitrogen-, fluorine-, and carbon-doping to TiO₂ to form mixed-anion materials, because it can easily prepare visible-light responsive photocatalysts [12]. Nitrogen doping into TiO₂ makes

impurity level at shallower potential than the valence band (VB) maximum of TiO₂ [13–18]. In the case of fluorine doping, Ti³⁺ is formed by reduction of Ti⁴⁺ as a counterpart of F[−] and the Ti³⁺ impurity level locates at deeper potential than the conduction band (CB) minimum of TiO₂ [18–20]. Carbon can be doped to both anionic and cationic sites of TiO₂ to form various types of impurity level between its band gap [15,18,21,22]. Such doping decrease excitation energy to induce visible-light responsivity. Because each dopant can lead to formation of different impurity level, we can design visible-light responsive TiO₂ with various band structures by selection or combination of various dopants. However, impurity level can sometimes work as a recombination centre, and its prevention is surely needed.

Formation of composite can suppress electron-hole recombination, because charge transfer can occur between two types of semiconductors with different band structures [23–25]. The excited electrons and holes transfer at the interface of composite can be categorized into two types; double-charge transfer mechanism and Z scheme mechanism. In the case of double-charge transfer mechanism (Scheme 1a), photoexcited electrons in CB of semiconductor B transfer to CB of semiconductor A, and photoexcited holes in VB of semiconductor A transfer to VB of semiconductor B. Because electrons and holes accumulate in CB of

* Corresponding author.

E-mail address: shuyin@tagen.tohoku.ac.jp (S. Yin).

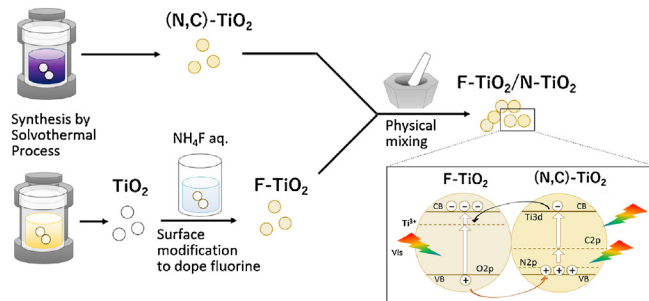


Scheme 1. Schematic diagram of electron–hole separation at the interface of composite; (a) double-charge transfer mechanism and (b) Z scheme mechanism.

semiconductor A and VB of semiconductor B, respectively, recombination between excited electrons and holes can be suppressed.

In the case of Z scheme mechanism (**Scheme 1b**), photoexcited electrons in CB of semiconductor A transfer to VB of semiconductor B, and combine with photoexcited holes in VB of semiconductor B. Consequently, electrons and holes are separated and accumulate in CB of semiconductor B and VB of semiconductor A, respectively. Recently, some semiconductors with doping have been applied as a component of such composites, and the composites have possessed distinguished photocatalytic activity [26–29]. However, effect of their impurity level induced by doping on catalytic activity of composites has not been understood exactly. Such understanding can enable to precisely design photocatalytic composite materials and these photoreaction processes.

In this study, we demonstrate the effect of impurity level of semiconductor on photocatalytic activity of composite. Anatase-type TiO_2 photocatalysts with anion doping were used as a component of photocatalyst composites. Because anatase-type TiO_2 with different dopants possess different impurity level with the same conduction and valence bands, we can easily focus only the effect of the impurity level. Three types of anatase-type TiO_2 doped with various anions, such as fluorine-doped TiO_2 (F- TiO_2), carbon-doped TiO_2 (C- TiO_2) and nitrogen and carbon-doped TiO_2 ((N,C)- TiO_2), were used as the component of photocatalyst composites; In addition, anatase-type TiO_2 without doping was also synthesized for comparison. By simply mixing any two of those materials, such as TiO_2 and (N,C)- TiO_2 ($\text{TiO}_2/\text{(N,C)-TiO}_2$), F- TiO_2 and (N,C)- TiO_2 (F- $\text{TiO}_2/\text{(N,C)-TiO}_2$), F- TiO_2 and C- TiO_2 (F- $\text{TiO}_2/\text{C-TiO}_2$), C- TiO_2 and (N,C)- TiO_2 (C- $\text{TiO}_2/\text{(N,C)-TiO}_2$), various kind of composites were prepared, and their photocatalytic NO_x decomposition activities were evaluated under visible- and UV light irradiation (**Scheme 2**). Because the photocatalytic activity of F- $\text{TiO}_2/\text{(N,C)-TiO}_2$ was higher than that of F- TiO_2 and (N,C)- TiO_2 , the carrier dynamics of the composite was analysed for understanding the role of their impurity levels. In addition, the effect of mixing ratio of F- $\text{TiO}_2/\text{(N,C)-TiO}_2$ on the photocatalytic activity was also investigated. From those results, we discussed about the photo-reaction process and the mechanism for the effect of impurity level on photocatalytic activity of the composite.



Scheme 2. Schematic synthesis flow of F- $\text{TiO}_2/\text{(N,C)-TiO}_2$.

2. Experimental

2.1. Synthesis of TiO_2 with and without doping and preparation of their composites

TiO_2 was synthesized by a solvothermal process. First, titanium tetraisopropoxide (Kanto Chemical Co., Inc., 1.2 mL) was added to a mixed solvent including ethanol (Kanto Chemical Co., Inc., 8 mL) and acetic acid (Kanto Chemical Co., Inc., 2 mL), and then stirred for 30 min. After that, the mixture was transferred to a Teflon container with internal volume of 100 mL, and the container was put in stainless steel autoclave. The autoclave was heated at 240 °C for 24 h with rotation at 100 rpm. After the treatment, the mixture was filtrated, and white powders were obtained. The white powders were washed with distilled water and ethanol, and dried at 60 °C overnight. The obtained sample was denoted as TiO_2 . F- TiO_2 was prepared by treatment of the obtained TiO_2 with ammonium fluoride (NH_4F) aqueous solution [30]. The obtained TiO_2 (7.2 g) was added to 0.11 M NH_4F aqueous solution (Kanto Chemical Co., Inc., 8 mL) and the dispersion was stirred for 24 h at room temperature. After the stirring, the dispersion was filtrated to obtain a white precursor. After washing and drying, the white powders were put into alumina crucible and calcined at 300 °C for 2 h in air to obtain a beige colour of sample, which was denoted as F- TiO_2 . (N,C)- TiO_2 was synthesized on the basis of our previous report [31]. A solution of 20 wt % Titanium (III) chloride (Kanto Chemical Co., Inc., 21.5 mL) and hexamethylenetetramine (Kanto Chemical Co., Inc., 10 g) were mixed with methanol (Wako Co., 25 mL). The mixture was transferred to a Teflon container in stainless steel autoclave, and heated at 190 °C for 2 h. After filtration, the sample was washed and dried overnight. The obtained beige powder was denoted as (N,C)- TiO_2 . C- TiO_2 was also synthesized on the basis of our other previous report [32]. Firstly, titanium(IV) tetrabutoxide (Kanto Chemical Co., Inc., 2.5 mL) was mixed with ethanol (8 mL) and then the mixture was stirred for 30 min. Then, a mixed solvent including ethanol (10 mL) and distilled water (15 mL) was added to the mixture, and stirred for 30 min. To carry out the solvothermal reaction, the mixture was introduced into a Teflon-sealed autoclave. After heating at 190 °C for 2 h, white powders as precursor for C- TiO_2 were obtained after filtration. The white powders were heated at 265 °C for 2 h in air to produce C- TiO_2 . For the preparation of various composites, any two kinds of TiO_2 -based single materials were physically mixed by using agate mortar. Four kinds of composites including F- $\text{TiO}_2/\text{(N,C)-TiO}_2$, F- $\text{TiO}_2/\text{TiO}_2$, (N,C)- $\text{TiO}_2/\text{C-TiO}_2$ and F- $\text{TiO}_2/\text{C-TiO}_2$ were obtained. Basically, the mixing ratio of the two materials in the composites was 1:1.

2.2. Characterization

The crystalline phases and crystallite size of samples were identified by powder X-ray diffraction analysis (XRD, Bruker AS, Inc., D2PHASER) using $\text{Cu K}\alpha$ radiation. The size and shape of the obtained samples were observed by transmission electron microscopy (TEM, JEOL Inc., JEM-2000EXII). The specific surface areas were calculated from N_2 absorption measurements by the BET equation (Quantachrome Instruments Japan LLC, NOVA 4200e). The UV-vis diffuse reflectance spectra (DRS) were measured by using a UV-vis spectrophotometer (JASCO Co., V-670). The composition and chemical bonding state of samples were detected by X-ray photoelectron spectroscopy (XPS, ULVAC-PHI, Inc., PHI5600).

2.3. Measurement of transient absorption spectra

Microsecond time-resolved visible to mid-IR absorption measurements were performed by using the custom-built spectrometers, as reported in our previous paper [33]. Briefly, in the mid-IR region ($6000 - 1000 \text{ cm}^{-1}$), the probe light emitted from an IR source was focused on the sample, and the transmitted light was monochromated

by a grating spectrometer. The output light intensity was converted to electric signal by an MCT detector (Kolmar Inc.), and the signal was amplified with an AC-coupled amplifier (Stanford Research Systems, SR560, 1 MHz). In the visible to NIR region ($25,000\text{--}6000\text{ cm}^{-1}$), a halogen lamp and Si (Thorlab Inc.) or InGaAs (Thorlab Inc.) photodiodes were utilized for the probe light source and detectors, respectively. In this wavenumber region, the experiments were performed in reflection mode. In the experiments, powder photocatalysts were fixed on a circular CaF_2 plate with density of 3 mg cm^{-1} and placed in the closed IR cell. The band gap of the photocatalysts was photoexcited by a 355 nm UV pulse from a Nd:YAG laser (Continuum, Surelite I, duration: 6 ns, power: 0.5 mJ pulse^{-1} , repetition rate: 5–0.1 Hz). Then the decay curve of the transient absorption at a fixed wavenumber was recorded by a digital oscilloscope (Lecroy). The time resolution of the spectrometers was limited to 1–2 μs by the bandwidth of the amplifier. All measurements were performed in a vacuum at room temperature.

2.4. Evaluation of photocatalytic activity

Photocatalytic deNO_x abilities of the obtained materials were evaluated based on our previous report [34]. Volume of the sample powders were unified by glass cell ($20\text{ mm} \times 16\text{ mm} \times 0.5\text{ mm}$). The glass cell with photocatalyst was put on the bottom of a flow type reactor. NO_x total concentration of the sample gas was set to 1.00 ppm by $\text{NO}(2\text{ ppm})/\text{N}_2$ gas mixed with compressed air. The mixed gas was introduced to the reactor with a flow rate of 200 mL min^{-1} . The NO_x concentration was measured by NO_x analyzer (YANACO Co., ECL-88AO Lite). The deNO_x ratio was defined by the follow equation.

$$\text{deNO}_x \text{ ratio (\%)} = \frac{C_0 - C}{C_0} \times 100$$

where C_0 is initial NO_x concentration in the mixed gas and C is the NO_x concentration after decomposition of NO_x by photocatalyst under 2 mW LED lights irradiation (627, 530, 445, 390 nm) at room temperature.

3. Results and discussion

3.1. Characterization of non-metal doped TiO_2 photocatalysts

The XRD patterns of the prepared samples matched well with that of anatase phase of TiO_2 (JCPDS No. 89-4921) (Fig. 1a). The TEM images showed that the prepared samples possessed aggregated structure of primary nanoparticles (Fig. 1b). The average crystallite sizes and the specific surface areas (SSA) of the samples were summarized in Table 1. All the prepared samples possessed high specific surface area compared with that of P25 (commercially obtained TiO_2 with high photocatalytic activity) ($\text{SSA} = 65\text{ m}^2/\text{g}$). The average crystallite size was calculated from the half width of (101) peak by the Scherrer equation (Scherrer constant: $K = 0.94$). The primary particle sizes observed in the TEM analysis were consistent with the calculated crystallite size. This result indicated that the primary particles were single crystals.

In both the XPS spectra of F- TiO_2 before and after Ar sputtering, the signal of fluorine (684 eV) was detected (Fig. 2a), indicating the presence of fluorine inside the F- TiO_2 [35]. The N1s (400 eV) and C1s (284 eV) signals were also detected in the F- TiO_2 . According to previous reports, these signals suggest the presence of surface chemisorbed nitrogen or carbon molecular species [36–39]. The N1s XPS spectra of (N,C)- TiO_2 after Ar sputtering showed the signal around 394 eV. The signal corresponded to the chemical bonding between nitrogen and Ti [36,37]. The N-Ti bonding in the (N,C)- TiO_2 strongly suggested the formation of nitrogen doping on the oxygen site. Additionally, the C1s XPS spectra of (N,C)- TiO_2 after Ar sputtering showed the signal at around 282 eV, corresponding to carbon bonded with Ti [38,39]. From the C1s XPS spectra of C- TiO_2 after Ar sputtering, the signal at around 282 eV was detected, indicating that carbon was doped on the oxygen site. These results indicated the successful doping during the mentioned

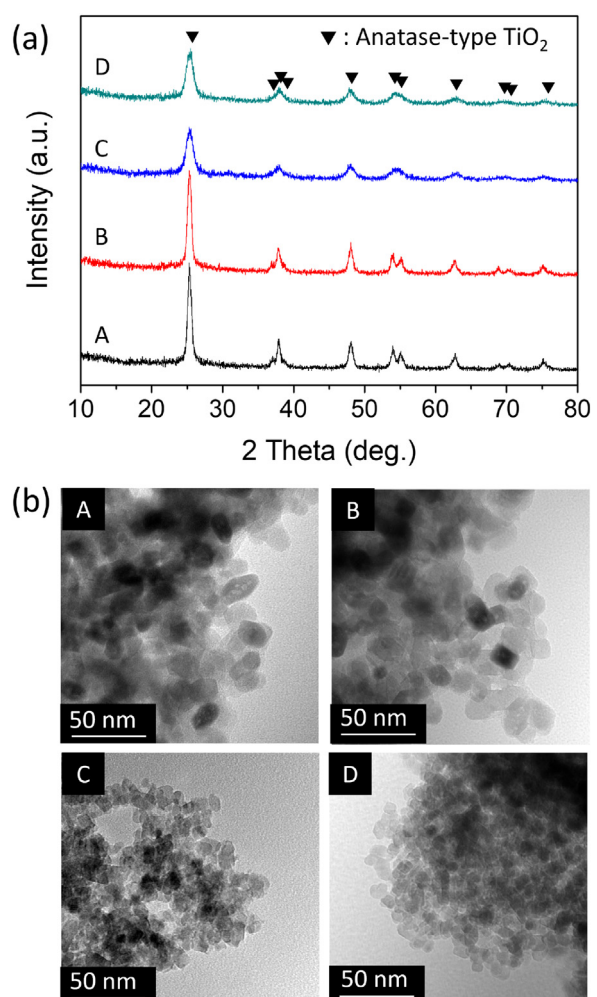


Fig. 1. (a) XRD patterns and (b) TEM images of (A) TiO_2 , (B) F- TiO_2 , (C) (N,C)- TiO_2 and (D) C- TiO_2 .

Table 1
Crystallite size and specific surface area of prepared samples.

Sample	Crystallite size (nm)	Specific surface area (m^2/g)
TiO_2	12	110
F- TiO_2	13	96
(N, C)- TiO_2	7.5	122
C- TiO_2	7.3	168

synthesis processes. The UV-vis-DRS spectra of F- TiO_2 , (N,C)- TiO_2 , and C- TiO_2 showed higher absorption under visible light range (380–620 nm) than that of TiO_2 (Fig. 2d). These results suggested that non-metal doping was effective for increase of visible light absorption probably because of the formation of impurity level in their band gap.

3.2. Photocatalytic deNO_x activity

Fig. 3 shows average photocatalytic NO_x decomposition (deNO_x) ratios on the prepared samples; TiO_2 , F- TiO_2 , (N,C)- TiO_2 , $\text{TiO}_2/(N,C)\text{-TiO}_2$ and F- $\text{TiO}_2/(N,C)\text{-TiO}_2$. The conversion ratios of F- TiO_2 and (N,C)- TiO_2 were higher than that of TiO_2 without doping, indicating that the F- or N-doping improved the visible-light induced photocatalytic activity (F- TiO_2 : $\lambda \geq 445\text{ nm}$, N- TiO_2 : $\lambda \geq 530\text{ nm}$). The composite F- $\text{TiO}_2/(N,C)\text{-TiO}_2$ exhibited further higher deNO_x activity than those of F- TiO_2 and (N,C)- TiO_2 under the visible-light irradiation ($\lambda \geq 445\text{ nm}$). On the other hand, $\text{TiO}_2/(N,C)\text{-TiO}_2$ did not exhibit improved visible-

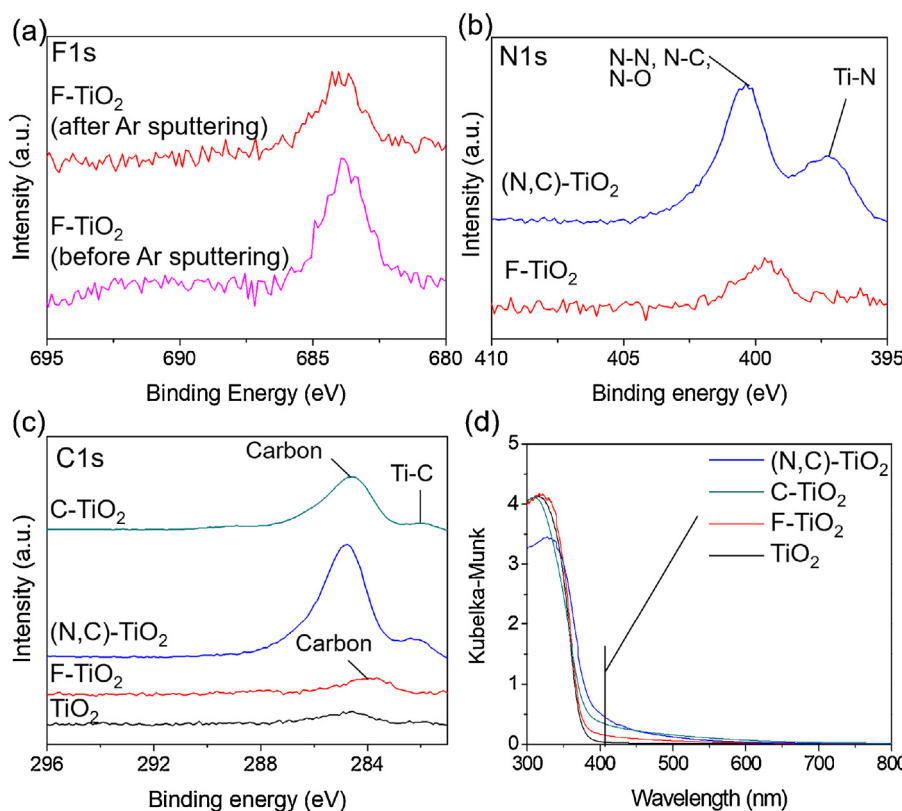


Fig. 2. (a) F1s spectra of F-TiO₂ before and after Ar sputtering, (b) N1s, (c) C1s spectra of prepared samples after Ar sputtering and (d) UV-vis DRS spectra of prepared samples.

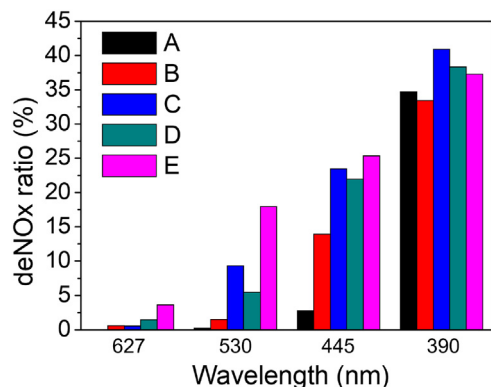


Fig. 3. Average deNO_x ratio of (A) TiO₂, (B) F-TiO₂, (C) (N,C)-TiO₂, (D) TiO₂/ (N,C)-TiO₂ and (E) F-TiO₂/ (N,C)-TiO₂.

light induced photocatalytic activity, suggesting that impurity level by F doping in F-TiO₂ could play a crucial role for the improvement of photocatalytic activity on the composite.

The effect of composite ratio of F-TiO₂/(N,C)-TiO₂ was investigated by changing the mixing ratio; F-TiO₂ : (N,C)-TiO₂ = 3 : 1 ((3 : 1) F-TiO₂/(N,C)-TiO₂), 1 : 1 (F-TiO₂/(N,C)-TiO₂) and 1 : 3 ((1 : 3) F-TiO₂/(N,C)-TiO₂). These photocatalytic activities were summarized in Fig. 4. F-TiO₂/(N,C)-TiO₂ showed the highest photocatalytic activity under visible light irradiation ($\lambda \geq 530$ nm). In addition, under blue light irradiation ($\lambda = 445$ nm), the photocatalytic activity of the three composites were almost the same. Therefore, the optimum mixing ratio of composite for the improvement of photocatalytic activity was 2 : 2.

The photo-induced deNO_x activity of C-TiO₂ and its composite with F-TiO₂ or (N,C)-TiO₂ were summarized in Fig. 5. Although C-TiO₂ showed high visible light photocatalytic activity, C-TiO₂/F-TiO₂ and C-

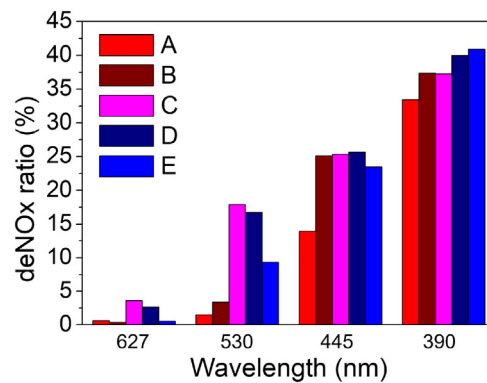


Fig. 4. Average deNO_x ratio of (A) F-TiO₂, (B) (3 : 1)F-TiO₂/(N,C)-TiO₂, (C) F-TiO₂/(N,C)-TiO₂, (D) (1 : 3)F-TiO₂/(N,C)-TiO₂ and (E) (N,C)-TiO₂.

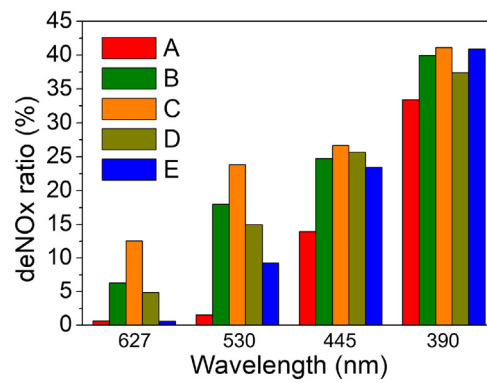


Fig. 5. Average deNO_x ratio of (A) F-TiO₂, (B) F-TiO₂/C-TiO₂, (C) C-TiO₂, (D) C-TiO₂/(N,C)-TiO₂ and (E) (N,C)-TiO₂.

$\text{TiO}_2/\text{(N,C)-TiO}_2$ did not possess enhanced photocatalytic activity compared with their pristine materials, suggesting that C-TiO_2 was not suitable for the improvement of photocatalytic activity in the composites. Consequently, only the combination between F-TiO_2 and (N,C)-TiO_2 improved the photocatalytic deNO_x activity, suggesting that both fluorine doping and nitrogen / carbon co-doping should be very important for the improvement of the photocatalytic activity.

3.3. Measurement of transient absorption spectra

According to the previous reports, trapping energy states of photo-excited carriers can be estimated from wavenumber region in which the absorption peaks/signals appear. [33,40–42]. A signal in the region of $3000\text{--}1000\text{ cm}^{-1}$ (3333–10000 nm) is mainly attributed to the absorption of free electrons and/or electrons at shallow trap levels located in the mid-gap ($\leq 0.4\text{ eV}$ deeper than conduction band minimum). On the other hand, a signal in the region around $20,000\text{ cm}^{-1}$ (500 nm) is mainly derived from absorption by holes and/or electrons at deep trap levels in the mid-gap. In fact, the decay kinetics at $20,000\text{ cm}^{-1}$ under various gases indicates that the signal intensity dominantly includes absorption by holes at deep trap levels (Fig. S1). Because the amount of F-TiO_2 and (N,C)-TiO_2 is equal in $\text{F-TiO}_2/\text{(N,C)-TiO}_2$, the absorption intensity of $\text{F-TiO}_2/\text{(N,C)-TiO}_2$ should be on the average of those of F-TiO_2 and (N,C)-TiO_2 . However, the transient absorbance of $\text{F-TiO}_2/\text{(N,C)-TiO}_2$ was obviously higher than those of F-TiO_2 and (N,C)-TiO_2 under almost all the measured wavenumber (Fig. S6a). These results indicated the number of surviving photoexcited electrons and holes of $\text{F-TiO}_2/\text{(N,C)-TiO}_2$ was larger than those of F-TiO_2 and N-TiO_2 .

The decay kinetics at 2000 and $20,000\text{ cm}^{-1}$ of F-TiO_2 , (N,C)-TiO_2 and $\text{F-TiO}_2/\text{(N,C)-TiO}_2$ were also measured (Fig. 6b,c). Because the transient absorptions at 2000 and $20,000\text{ cm}^{-1}$ were assigned to electrons and holes, respectively, as mentioned above, the decay kinetics at 2000 and $20,000\text{ cm}^{-1}$ showed the lifetime of electrons and holes, respectively. It is evident from Fig. 6c that the lifetime of holes is longer in the $\text{F-TiO}_2/\text{(N,C)-TiO}_2$ than those of F-TiO_2 and (N,C)-TiO_2 , suggesting that the charge separation is enhanced by the physical mixing. In the case of free electrons, their lifetime in the composite is apparently comparable to F-TiO_2 but still longer than (N,C)-TiO_2 (Fig. 6b). If the charge transfer does not proceed among the particles, the number of surviving free electrons should be the simple average in F-TiO_2 and (N,C)-TiO_2 : the decay curves should be located in the middle between F-TiO_2 and (N,C)-TiO_2 . Therefore, the comparable intensity with F-TiO_2 is supporting that the charge separation is also enhanced for free electrons. The longer life time of electrons and holes in the $\text{F-TiO}_2/\text{(N,C)-TiO}_2$ composite clearly suggests that recombination between photoexcited electrons and holes is suppressed and hence enhancing its photocatalytic activity.

3.4. Discussion about mechanism for the improvement of photocatalytic activity of $\text{F-TiO}_2/\text{(N,C)-TiO}_2$

Here, we discuss the mechanism for the photocatalytic improvement, or the long lifetime of the photoexcited carries in the composite $\text{F-TiO}_2/\text{(N,C)-TiO}_2$. Both F-TiO_2 and (N,C)-TiO_2 with anatase phase possessed different doping levels with almost the same valence and conduction band positions. Therefore, we must consider the effect of the impurity levels by doping in the composite. In F-TiO_2 , Ti^{3+} induced by reduction of Ti^{4+} exists as a counterpart of F^- to form an inter-band gap level at slightly deeper position than the TiO_2 conduction band minimum [17–19]. The inter-band gap level leads to photoexcitation under visible-light irradiation and the subsequent photocatalytic reaction. In fact, F-TiO_2 possessed high photocatalytic activity under blue and UV light irradiation ($\lambda = 445$ and 390 nm) (Fig. 3(B)). On the other hand, (N,C)-TiO_2 possesses two impurity levels derived from N- and C-doping. The level by N-doping locates on the slightly shallower position than valence band maximum, and the level by C-doping locates on the

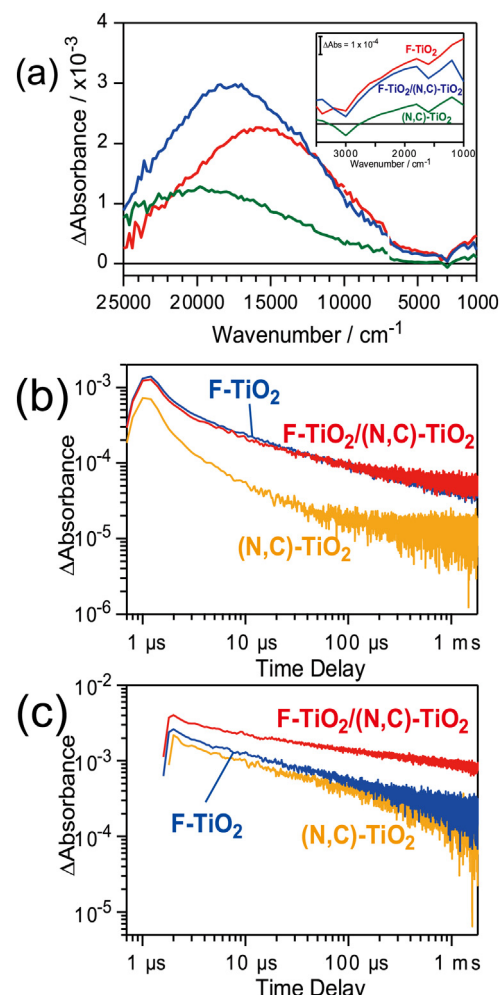


Fig. 6. (a) Transient absorption spectra measured at $5\text{ }\mu\text{s}$ after UV pulse laser irradiation, (b) and (c) their decay kinetics at (a) 2000 cm^{-1} and (b) $20,000\text{ cm}^{-1}$ of F-TiO_2 , (N,C)-TiO_2 and $\text{F-TiO}_2/\text{(N,C)-TiO}_2$.

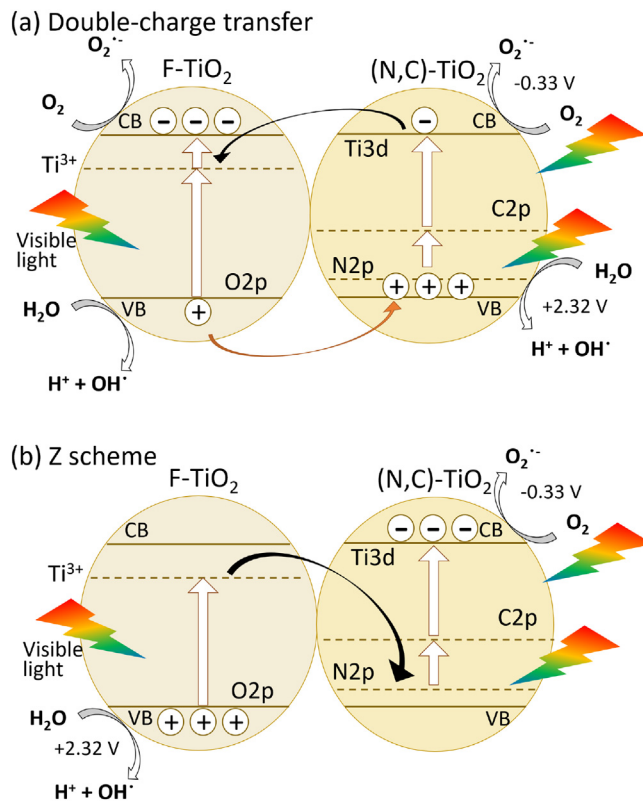
middle of band gap. By the impurity levels, (N,C)-TiO_2 possessed visible-light photocatalytic deNO_x activity (Fig. 3(C)).

Generally, photocatalytic NO_x decomposition mechanism proceeds by following reaction equations [43].



Actual photocatalytic reactions are the Eqs. (2) and (3). Therefore, the relationship between the redox potentials of $\text{O}_2/\text{O}_2^\cdot$ and $\text{H}_2\text{O}/\text{OH}^\cdot$ and the potentials of holes and electrons in semiconductor photocatalysts are essential for the progress of this reactions. Considering the redox potentials of $\text{O}_2/\text{O}_2^\cdot$ (-0.33 eV) and $\text{H}_2\text{O}/\text{OH}^\cdot$ (+2.32 eV), holes or electrons in the doping level of F-TiO_2 and (N,C)-TiO_2 cannot exhibit the (2) or (3) reactions, respectively [44]. Therefore, holes and electrons in the valence and conduction band must be utilized for the reactions (2) and (3).

According to these facts shown above, two possible mechanism can be proposed for the photocatalytic NO_x decomposition in the composite $\text{F-TiO}_2/\text{(N,C)-TiO}_2$; (i) double charge transfer mechanism and (ii) Z-scheme mechanism. (i) The proposed process on the double charge



Scheme 3. Schematic illustration of the band structure and charge transfer type photoreaction process of $\text{F-TiO}_2/\text{(N,C)-TiO}_2$: (a) Double-charge transfer mechanism and (b) Z scheme mechanism.

transfer mechanism are shown in **Scheme 3a**. Photoexcited holes in F-TiO_2 moves to the impurity level by N-doping in $(\text{N,C})\text{-TiO}_2$, while photoexcited electrons in $(\text{N,C})\text{-TiO}_2$ moves to the Ti^{3+} 3d impurity level in F-TiO_2 . In addition, the electrons trapped in the Ti^{3+} 3d impurity level are further photo-excited into the conduction band of F-TiO_2 , and the holes trapped in the N impurity level in $(\text{N,C})\text{-TiO}_2$ also moves to the valence band of $(\text{N,C})\text{-TiO}_2$ by photoexcitation. Finally, the holes and electrons accumulates in the valence band of $(\text{N,C})\text{-TiO}_2$ and the electrons in the conduction band of F-TiO_2 , respectively, to make the photoexcited carriers spatially separated. The spatial separation can lead to suppress of recombination between photoexcited carriers, and can lengthen the carrier lifetimes. (ii) The proposed process on the Z-Scheme mechanism is shown in **Scheme 3B**. Under light irradiation, photoexcited electrons in Ti^{3+} 3d impurity level of F-TiO_2 compensate photoexcited holes in the valence band, the N impurity level or the C impurity level of $(\text{N,C})\text{-TiO}_2$. Consequently, photoexcited holes and electrons reach to the valence band of F-TiO_2 and the conduction band of $(\text{N,C})\text{-TiO}_2$, respectively, to make the photoexcited carriers spatially separated. The spatial separation can also lead to suppress of recombination between photoexcited carriers, and can lengthen the carrier lifetimes.

In the mechanism (ii), when F-TiO_2 is not photoexcited, photocatalytic NO_x decomposition must not be improved because of no spatial separation of photoexcited carriers in $(\text{N,C})\text{-TiO}_2$. However, the photocatalytic NO_x decomposition improved, when green light ($\lambda = 530 \text{ nm}$) which cannot excite F-TiO_2 was used (see the result in **Fig. 3**). On the other hand, the mechanism (i) can induce spatial separation of carriers photoexcited in $(\text{N,C})\text{-TiO}_2$. Even if the photoexcitation from the valence band to Ti^{3+} 3d impurity level in F-TiO_2 does not occur, the photoexcited electrons in $(\text{N,C})\text{-TiO}_2$ can transfer to the Ti^{3+} 3d impurity in F-TiO_2 , and can be further excited into the conduction band of F-TiO_2 to make the photoexcited carries spatially separated. Therefore, the mechanism (i) should work at least under the

green light irradiation ($\lambda = 530 \text{ nm}$). In the case of longer wavelength irradiation, the mechanism (i) may be dominant, although the two mechanisms compete.

In the case of the $\text{F-TiO}_2/\text{C-TiO}_2$ composite, no enhancement of photocatalytic activity was observed (**Fig. 5-(B)**). The positions of VB maximum of F-TiO_2 and C-TiO_2 are at very similar potential. Therefore, when we think the double-charge transfer mechanism for this case, photoexcited holes in $\text{F-TiO}_2/\text{C-TiO}_2$ cannot accumulate in VB of one semiconductor. Additionally, even if we assume the Z-Scheme mechanism, compensation of photoexcited electrons in F-TiO_2 with photoexcited holes in C-TiO_2 (recombination), because of the hole-electron reaction in the one semiconductor (F-TiO_2) and the energetically same between the VB maximum levels of F-TiO_2 and C-TiO_2 . Therefore, the composite should not possess improved effect.

The $\text{C-TiO}_2/(\text{N,C})\text{-TiO}_2$ composite did not also exhibit enhanced photocatalytic de NO_x activity (**Fig. 5-(D)**). The positions of CB minimum of C-TiO_2 and $(\text{N,C})\text{-TiO}_2$ are almost the same. Being similar to the case of $\text{F-TiO}_2/\text{C-TiO}_2$, photoexcited electrons in $\text{C-TiO}_2/(\text{N,C})\text{-TiO}_2$ cannot accumulate in CB of one semiconductor, if we think the double-charge transfer mechanism. On the other hand, when we assume Z-scheme mechanism for $\text{C-TiO}_2/(\text{N,C})\text{-TiO}_2$, the photocatalytic activity can be enhanced through compensation of photoexcited holes in N-impurity level of $(\text{N,C})\text{-TiO}_2$ with photoexcited electrons in CB of C-TiO_2 . However, the enhancement was not observed. This suggests that the $\text{C-TiO}_2/(\text{N,C})\text{-TiO}_2$ cannot exhibit Z-scheme process. This may suggest that Z-scheme process cannot easily work in this kind of composite. Because the moving way of electron and holes in the hypothesized Z-scheme process of $\text{C-TiO}_2/(\text{N,C})\text{-TiO}_2$ is very similar to that of $\text{F-TiO}_2/(\text{N,C})\text{-TiO}_2$, which may not exhibit Z-scheme process also.

Consequently, only the $\text{F-TiO}_2/(\text{N,C})\text{-TiO}_2$ composite exhibited the enhanced photocatalytic de NO_x activity, although we cannot understand the detail mechanism for the $\text{F-TiO}_2/(\text{N,C})\text{-TiO}_2$ composite at the present moment. Judging from the behaviours of the other composites, we think that the enhancement of the $\text{F-TiO}_2/(\text{N,C})\text{-TiO}_2$ composite may be explained by the double-charge transfer mechanism.

4. Conclusions

Composite of F-TiO_2 and $(\text{N,C})\text{-TiO}_2$ ($\text{F-TiO}_2/(\text{N,C})\text{-TiO}_2$) was prepared by simple physical mixing to exhibit higher visible-light responsive photocatalytic nitrogen oxide (NO_x) decomposition activity compared with those of F-TiO_2 and $(\text{N,C})\text{-TiO}_2$. The transient absorption spectra of F-TiO_2 , $(\text{N,C})\text{-TiO}_2$, and $\text{F-TiO}_2/(\text{N,C})\text{-TiO}_2$ and their decay kinetics showed that $\text{F-TiO}_2/(\text{N,C})\text{-TiO}_2$ possessed larger amount of photoexcited electrons and holes under light irradiation, and longer lifetime of the excited carries than those in F-TiO_2 and $(\text{N,C})\text{-TiO}_2$. The results strongly supported the effectiveness of the composite formation of doped TiO_2 for high visible-light responsive photocatalytic activity. The mechanism for the photocatalytic enhancement could be explained by the charge transfer between F-TiO_2 and $(\text{N,C})\text{-TiO}_2$ through their impurity levels. The charge transfer might be under the double-charge transfer mechanism, although we cannot deny charge transfer by the Z-scheme mechanism. Judging from no enhancement of photocatalytic de NO_x activity on the other composites, the impurity level by doping played a crucial role for the charge transfer. This indicated the possibility of the composite photocatalysts composed of different kind of doping materials. Although some oxides exhibit high visible-light responsive photocatalytic activity without doping, application of the strategy here by combination of doping and composite formation to such materials can further increase the visible-light induced photocatalytic activity.

Acknowledgements

This work was supported by the JSPS Grant-in-Aid for Scientific

Research on Innovative Areas “Mixed anion” (No. 16H06439, No. 17H05491) and for Young Scientists (B) (No. 17K14542), and by the Dynamic Alliance for Open Innovation Bridging Human, Environment and Materials in Network Joint Research Center for Materials and Devices.

Appendix A. Supplementary data

Supplementary material related to this article can be found, in the online version, at doi:<https://doi.org/10.1016/j.apcatb.2018.07.038>.

References

- [1] A. Fujishima, K. Honda, *Nature* 238 (1972) 37–38.
- [2] A. Kudo, Y. Miseki, *Chem. Soc. Rev.* 38 (2009) 253–278.
- [3] C. Chen, W. Ma, J. Zhao, *Chem. Soc. Rev.* 39 (2010) 4206–4219.
- [4] A. Fujishima, X. Zhang, D.A. Tryk, *Surf. Sci. Rep.* 63 (2008) 515–582.
- [5] O. Carp, C.L. Huisman, A. Reller, *Progress Solid State Chem.* 32 (2004) 33–177.
- [6] P.D. Tran, L.H. Wong, J. Barberbed, J.S.C. Loo, *Energy Environ. Sci.* 5 (2012) 5902–5918.
- [7] M. Pelaiza, N.T. Nolanb, S.C. Pillai, M.K. Seeryc, P. Falarasd, A.G. Kontosd, P.S.M. Dunlop, J.W.J. Hamilton, J.A. Byrnee, K. O'Sheaf, M.H. Entezarig, D.D. Dionysioua, *Appl. Catal. B Environ.* 125 (2012) 331–349.
- [8] K. Nagaveni, M.S. Hegde, G. Madras, *J. Phys. Chem. B* 108 (2004) 20204–20212.
- [9] L.G. Deviand, R. Kavitha, *Appl. Catal. B-Environ.* 140–141 (2013) 559–587.
- [10] S. Banerjee, S.C. Pillai, P. Falaras, K.E. O'Shea, J.A. Byrne, D.D. Dionysiou, *J. Phys. Chem. Lett.* 5 (2014) 2543–2554.
- [11] J. Choi, H. Park, M.R. Hoffmann, *J. Phys. Chem. C* 114 (2010) 783–792.
- [12] H. Kageyama, K. Hayashi, K. Maeda, J.P. Attfield, Z. Hiroi, J.M. Rondinelli, K.R. Poeppelmeier, *Nat. Commun.* 9 (772) (2018) 1–15.
- [13] C.W. Dunnill, I.P. Parkin, *Dalton Trans.* 40 (2011) 1635–1640.
- [14] C.D. Valentini, G. Pacchioni, A. Selloni, S. Livraghi, E. Giannello, *J. Phys. Chem. B* 109 (2005) 114114–114119.
- [15] R. Asahi, T. Morikawa, T. Ohwaki, K. Aoki, Y. Taga, *Science* 293 (13) (2001) 269–271.
- [16] R. Asahi, T. Morikawa, H. Irie, T. Ohwaki, *Chem. Rev.* 114 (2014) 9824–9852.
- [17] H. Irie, Y. Watanabe, K. Hashimoto, *J. Phys. Chem. B* 107 (2003) 5483–5486.
- [18] C.D. Valentini, G. Pacchioni, *Catal. Today* 206 (2013) 12–18.
- [19] W. Wang, C. Lu, Y. Ni, M. Su, Z. Xu, *Appl. Catal. B-Environ.* 127 (2012) 28–35.
- [20] C.D. Valentini, G. Pacchioni, *J. Phys. Chem. C* 113 (2009) 20543–20552.
- [21] C.D. Valentini, G. Pacchioni, A. Selloni, *Chem. Mater.* 17 (2005) 6656–6665.
- [22] G. Wu, T. Nishikawa, B. Ohtani, A. Chen, *Chem. Mater.* 19 (2007) 4530–4537.
- [23] J. Low, J. Yu, M. Jaroniec, S. Wageh, A.A. Al-Ghamdi, *Adv. Mater.* 29 (2017) 1601694.
- [24] P. Zhou, J. Yu, M. Jaroniec, *Adv. Mater.* 26 (2014) 4920–4935.
- [25] Y. He, L. Zhang, X. Wang, Y. Wu, H. Lin, L. Zhao, W. Weng, H. Wand, M. Fan, *RSC Adv.* 4 (2014) 13610–13619.
- [26] I. Kang, Q. Zhang, S. Yin, T. Sato, F. Saito, *Environ. Sci. Technol.* 42 (2008) 3622–3626.
- [27] X. Wu, S. Yin, Q. Dong, T. Sato, *Phys. Chem. Chem. Phys.* 15 (2013) 20633–20640.
- [28] H. Chuai, D. Zhou, X. Zhu, Z. Li, W. Huang, *Chin. J. Catal.* 36 (2015) 2194–2202.
- [29] A. Iwase, A. Kudo, *Chem. Commun.* 53 (2017) 6156–6159.
- [30] Y. Yu, H. Wu, B. Zhu, S. Wang, W. Huang, S. Wu, S. Zhang, *Catal. Lett.* 121 (2008) 165–171.
- [31] S. Yin, Y. Aita, M. Komatsu, J. Wang, Q. Tang, T. Sato, *J. Mater. Chem.* 15 (2005) 674–682.
- [32] X. Wu, S. Yin, Q. Dong, C. Guo, T. Kimura, J. Matsushita, T. Sato, *J. Phys. Chem. C* 117 (2013) 8345–8352.
- [33] A. Yamakata, M. Kawaguchi, N. Nishimura, T. Minegishi, J. Kubota, K. Domen, *J. Phys. Chem. C* 118 (41) (2014) 23897–23906.
- [34] S. Yin, B. Liu, P. Zhang, T. Morikawa, K. Yamanaka, T. Sato, *J. Phys. Chem. C* 112 (2008) 12425–12431.
- [35] H. Park, W. Choi, *J. Phys. Chem. B* 108 (13) (2004) 4086–4093.
- [36] N.C. Saha, H.G. Tompkins, *J. Appl. Phys.* 72 (7) (1992) 3072.
- [37] H. Irie, Y. Watanabe, K. Hashimoto, *J. Phys. Chem. B* 107 (2003) 5483–5486.
- [38] H. Irie, Y. Watanabe, K. Hashimoto, *Chem. Lett.* 32 (8) (2003) 772–773.
- [39] L. Zhang, R.V. Koka, *Mater. Chem. Phys.* 57 (1998) 23–32.
- [40] A. Yamakata, J.J.M. Vequizo, H. Matsunaga, *J. Phys. Chem. C* 119 (2015) 24538–24545.
- [41] A. Yamakata, M. Kawaguchi, R. Murachi, M. Okawa, I. Kamiya, *J. Phys. Chem. C* 120 (2016) 7997–8004.
- [42] A. Yamakata, J.J.M. Vequizo, M. Kawaguchi, *J. Phys. Chem. C* 119 (2015) 1880–1885.
- [43] J. Laseka, Y. Yua, J.C.S. Wua, *J. Photochem. Photobiol. C* 14 (2013) 29–52.
- [44] P.M. Wood, *Biochem. J.* 253 (1988) 287–289.